

Sintering, oxidation, and chemical properties of size-selected nickel clusters on TiO₂(110)

Masato Aizawa, Sungsik Lee, and Scott L. Anderson^{a)}
Department of Chemistry, University of Utah, Salt Lake City, Utah 84112

(Received 11 March 2002; accepted 12 June 2002)

We report a study of Ni_n/TiO₂ samples prepared by size-selected deposition of Ni_n⁺ ($n = 1, 2, 5, 10, 15$) on rutile TiO₂(110). The effects of deposition energy and support preparation conditions on the oxidation state of the clusters are examined by x-ray photoelectron spectroscopy (XPS). On the stoichiometric surface, Ni_n is stable, but oxidation can be driven by increased impact energy. For TiO₂ surfaces with chemisorbed oxygen, deposited Ni_n are oxidized even at low impact energies. Low energy ion scattering spectroscopy was used to characterize the dispersion of Ni on the support, and provide some insight into binding morphology. Small clusters bind preferentially to oxygen sites. Large clusters bind in compact geometries and appear to retain some three dimensional character on the surface. The data suggest that the clusters neither fragment, nor agglomerate, in room temperature deposition. Temperature programmed desorption (TPD) of CO was used to characterize deposited clusters. For these small clusters, no strong desorption features are observed in the temperature range above 140 K, where CO desorbs from TiO₂. The lack of CO binding is discussed in terms of strong Ni–TiO₂ binding. The ion scattering data indicate that there is significant sintering, and possibly partial encapsulation, of the Ni clusters during the TPD experiments. XPS reveals little change in oxidation state. This is the first study where the oxidation state and morphology of size-selected deposited clusters has been studied, before and after TPD.
© 2002 American Institute of Physics. [DOI: 10.1063/1.1498477]

I. INTRODUCTION

Deposition of mass-selected metal clusters on metal oxide supports has been shown by Heiz and co-workers to be an important tool for studying the effects of cluster size and support defects on catalytic activity.^{1–5} Recently they have shown a size dependence for the interaction of CO with Ni_n ($n < 30$) supported on ultrathin MgO (110) films, using temperature programmed desorption (TPD) and infrared spectroscopy.^{2,3} The binding of CO to Ni clusters on MgO is strong, as shown by the appearance of nickel carbonyl species in the thermal desorption mass spectra for the small clusters ($n < 4$). Only CO desorption is observed for the larger clusters (Ni_n, $n = 11, 20$, and 30). They found two types of CO adsorption sites. On one, CO chemisorbs molecularly, resulting in a desorption between 200–300 K. On the second site, CO is dissociated and desorbs associatively between 500–600 K.

We recently built an instrument that allows us to investigate physical and chemical properties of mass-selected metal clusters deposited on metal oxides. The capabilities are somewhat complementary to those of Heiz and co-workers, including TPD, x-ray photoelectron spectroscopy (XPS), and ion-scattering spectroscopy (ISS), but not infrared spectroscopy. The inclusion of ISS is important, because it provides a measure of changes in cluster morphology with deposition energy, cluster size, and following TPD. Here we report a study of oxidation, sintering, and CO-adsorption behavior of

Ni_n deposited on TiO₂ at different deposition energies, and with different TiO₂ preparation conditions. For comparison, we also studied Ni particles grown by deposition of a 1.0 ML dose of nickel atoms. TiO₂ was chosen as the initial support for study because we wanted a system where the metal-support binding would be strong enough to minimize diffusion and sintering of the deposited clusters at room temperature. The results are quite different from the behavior observed by Heiz and co-workers on MgO, reflecting the much stronger Ni-support binding for TiO₂.

There are a number of motivations for studying the Ni/TiO₂ system. Nickel particles supported on TiO₂ are used in heterogeneous catalysis. In addition, the rutile TiO₂(110) surface has been studied extensively, and there are a number of studies addressing the morphology and electronic properties of Ni evaporated onto TiO₂(110), useful in interpreting our results. The structure of the surface is shown in Fig. 1, along with several possible binding motifs for Ni₂ and Ni₅. The surface unit cell is indicated by the white rectangle, and the density of unit cells is $\sim 7 \times 10^{14}/\text{cm}^2$. Also indicated with circled letters A–D, are the Ni binding sites identified by Pala, Liu, and Truong⁶ in recent density functional calculations. The binding energies are 2.6, 2.0, 1.8, and 0.6 eV, for A–D, respectively. In these periodic calculations, there is one Ni atom per surface unit cell, and it is unclear how the binding energies might change with coverage. Nonetheless, their results indicate that Ni–TiO₂ binding is both relatively strong, and quite corrugated (i.e., site-dependent).

A number of groups have also reported experimental

^{a)}Electronic mail: anderson@chem.utah.edu

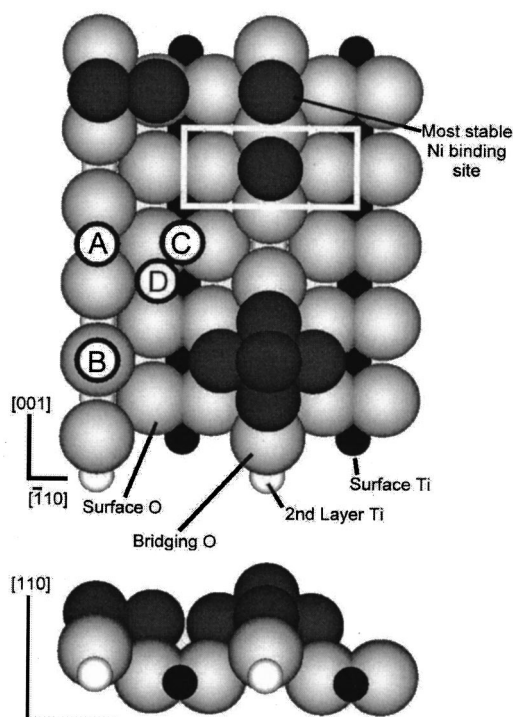


FIG. 1. The structure of the rutile $\text{TiO}_2(110)$ surface, showing surface and second layer Ti, surface and bridging O. The surface unit cell is indicated as a white rectangle. A–D indicate the Ni binding sites calculated by Pala *et al.* (Ref. 6) in order of decreasing stability. The dark spheres indicate the potential Ni dimer and Ni_5 binding arrangements.

studies of Ni evaporated onto $\text{TiO}_2(110)$. Onishi *et al.*,⁷ on the basis of the Ni dose-dependence of Auger intensities, concluded that Ni grows as a surface layer for densities up to $\sim 8 \times 10^{14}/\text{cm}^2$ (i.e., \sim one Ni/unit cell), then begins to form three-dimensional structures. Other authors conclude that growth is three-dimensional (Volmer–Weber) even at low coverages.^{8,9} In STM, cluster morphology is clearly seen at low coverages ($\sim 2 \times 10^{14}$ Ni/cm²) following deposition at 375 K.⁸ The origin of the discrepancy is unclear, but may be related to dose rate or surface conditions. One problem in comparing with these earlier studies is that they all use different methods for TiO_2 preparation, and it is not clear that the support is identical.

The metal-support electronic interactions of nickel particles formed during Ni evaporation onto $\text{TiO}_2(110)$ have been studied by electron spectroscopy.^{7,9–11} On stoichiometric $\text{TiO}_2(110)-(1 \times 1)$, only the zero oxidation state Ni is observed, however, the Ni $2p$ binding energy is observed to increase with decreasing nickel coverage. This shift has been explained in terms of final state relaxation effects, and Kao *et al.*¹⁰ also proposed that there is partial electron transfer ($\sim 0.13 e^-/\text{Ni}$) from TiO_2 to Ni. This last point is contradicted by the work function measurements of Onishi *et al.*,⁷ which were interpreted to indicate a $\sim 0.1 e^-/\text{Ni}$ electron transfer from Ni to TiO_2 . CO desorption temperatures have also been reported by Raupp and Dumesic¹² for nanometer size nickel particles formed by Ni evaporation onto $\text{TiO}_2(110)$. It was found that the desorption peak shifts to decreasing temperatures with decreasing Ni evaporative dose, and with increasing density of missing-oxygen defects

on the TiO_2 . Finally, on the basis of decreasing Ni XPS signal following extended annealing, Kao *et al.*¹⁰ inferred that Ni diffuses into the TiO_2 bulk at elevated temperatures. This conclusion is contradicted by the more recent XPS and ISS work of Espinós *et al.*¹¹ who observed no Ni signal loss for stoichiometric TiO_2 , but did observe diffusion into the bulk for defective TiO_x prepared by Ar^+ sputtering.

II. EXPERIMENT

The instrument consists of a cluster source, a mass-selecting beamline, and a set of UHV chambers where deposition, sample preparation, and analysis are carried out. The beamline and sample handling arrangement have been described in previously.^{13,14} Nickel cluster ions are generated by a 100 Hz laser vaporization source, similar to the source recently reported by Heiz and co-workers.¹⁵ A 100 Hz Nd:YAG laser (Spectra Physics) is tightly focused on a rectangular nickel target that is continuously rastered under computer control. The vaporized metal plasma is entrained in a pulsed helium flow and swept down a 1.5 mm diameter channel, where cluster ions grow. At the end of the channel, the gas pulse exits through a nozzle, and cluster ions are injected into a 27 cm long quadrupole ion guide. At the end of this first guide, the cluster ion beam is deflected by 18° and injected into a second quadrupole which guides the ions through several more differential pumping walls, and delivers them to a commercial quadrupole mass filter (Extrel). After mass selection, the clusters are guided by a final quadrupole into the UHV section of the instrument, where they are deposited on the room temperature substrate through a 2 mm diam mask/lens.

The cluster dose is measured by continuously monitoring current on the target, and unless indicated otherwise, the coverage was always 2.0×10^{14} Ni atoms per cm², equivalent to a tenth of a close-packed Ni monolayer. The impact energy was varied by floating the beamline potentials with respect to the grounded TiO_2 target. Typical intensities of mass-selected cluster ions, delivered to the deposition substrate, range from 1 to 25 nA/cm². Deposition times are typically 30–60 min. The deposition energy distribution is estimated by retarding potential analysis on the deposition target, i.e., measurement of the drop in deposition current as the target potential is raised. Because the target current is effected by beam divergence and space charge, as well as the energy spread, the energy width extracted from retarding analysis is approximate, and should be an upper limit. The full width at half maximum of the energy width is < 1 eV, for all cluster sizes. The base pressure in the UHV system is $\sim 1 \times 10^{-10}$ Torr. The pressure in the deposition chamber rises to $\sim 2 \times 10^{-9}$ Torr during deposition, however, the additional gas is ultrahigh purity helium from the laser vaporization source. Contamination of the surface is routinely monitored before and after experimental runs. For this system, there is no evidence for reaction with background gases on the experimental time scale.

The UHV system is equipped with a hemispherical energy analyzer, a dual anode x-ray source (here, using $\text{Al K}\alpha$ radiation) and an ion gun, allowing sample characterization

by x-ray photoelectron spectroscopy (XPS) and low energy ion scattering spectroscopy (ISS). The sample can be transferred into a separate UHV chamber for temperature-programmed desorption (TPD) studies. For TPD, the sample was heated at 3 K/s by electron bombardment from the backside. Desorbing molecules enter the differentially pumped quadrupole mass spectrometer through a 2 mm diameter aperture in the end of a conical skimmer. The aperture matches our deposition spot size, and is positioned ~ 1 mm from the TiO_2 substrate, minimizing desorption background from other surfaces. Samples are cleaned by Ar^+ sputtering, then annealed in one of two stations. One is used for annealing in UHV, and the other, located in a separate chamber, allows annealing at high O_2 pressures.

XPS spectra were used to estimate TiO_2 stoichiometries for the near-surface region. The spectra were corrected using Shirley background subtraction,¹⁶ before the XPS peak areas were integrated. Atomic sensitivity factors for our instrumental configuration were taken from the PHI Handbook.¹⁷ We note that the binding energies of $\text{Ti } 2p$ and $\text{O } 1s$ differ by only 70 eV, so that the corresponding electron kinetic energies differ by only $\sim 7\%$. As a consequence, the usual uncertainties arising from energy-dependence electron detection efficiency should be minimal. The stoichiometries derived from XPS reflect average properties of a near-surface region defined by the inelastic mean free path (λ) for electrons in TiO_2 . For $\text{O } 1s$ and $\text{Ti } 2p$ photoelectrons λ is ~ 21 Å, while for $\text{Ni } 2p$ photoelectrons λ is ~ 14 Å.¹⁸

$\text{TiO}_2(110)$ single crystals (Commercial Crystal Laboratories) are mounted on a homebuilt sample holder¹⁴ that allows samples to be moved between different preparation or analysis stations with precise positioning. The crystal is clamped against a thick molybdenum backing plate that can be cooled by conduction to a liquid N_2 reservoir. For TPD or annealing in vacuum, the metal backing plate is heated by electron bombardment from the back side. For lower temperature annealing in O_2 atmospheres, the entire sample holder is heated by conduction from a resistively heated copper stage. The crystal temperature is measured by a thermocouple bonded inside a slot cut into the edge of the TiO_2 crystal, using UHV-compatible cement. In order to make the crystal conductive enough to allow ion deposition and minimize charging in XPS, the crystal was initially annealed in UHV at 1000 K for 1 h. This process creates defects throughout the bulk, and results in n -type semiconducting properties reflected in a permanent color change from the initially transparent crystal. The main surface contaminant is Na, which is present at ppm concentrations in the TiO_2 bulk, and also a component of the ceramic cement (AREMCO 571) used to bond the thermocouple. Freshly mounted crystals are subjected to repeated sputter/anneal cycles until negligible contaminant signal is observed by ISS and XPS, ISS being extremely sensitive to surface Na. Following each cluster deposition experiment, the crystal was sputtered with 1 kV Ar^+ ions well past the point where no Ni XPS or ISS signal was observed, and the regular sputtering also prevented re-appearance of alkali contamination. The sample was then annealed under different conditions to generate titania with desired surface properties.

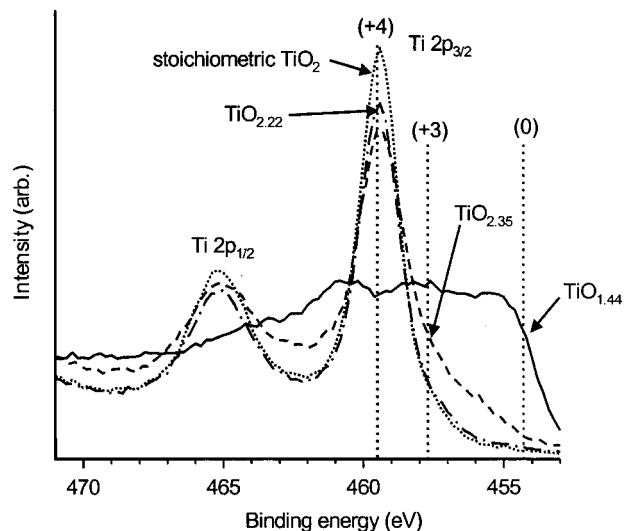


FIG. 2. The $\text{Ti } 2p$ XPS of clean TiO_2 under different preparation conditions. “ $\text{TiO}_{1.44}$ ” is the surface following Ar^+ ion sputtering only. “ TiO_2 ” is sputtered then annealed in UHV at 900 K. “ $\text{TiO}_{2.35}$ ” is sputtered then annealed in O_2 at 570 K. “ $\text{TiO}_{2.22}$ ” is sputtered then annealed in O_2 at 700 K. The vertical dashed lines indicate the expected binding energies for Ti in different oxidation states.

III. RESULTS AND DISCUSSION

Ni_2^+ , Ni_5^+ , and Ni_{10}^+ were deposited at impact energies of 1 eV/atom and 10 eV/atom, always with the dose equivalent to 0.1 ML of atoms (2.0×10^{14} atoms/cm²). Several experiments were also run with Ni^+ and Ni_{15}^+ at 1 eV/atom. The XPS of the as-deposited sample was used to characterize the distribution of oxidation states of Ni and Ti, and ISS was used to characterize the morphology of the sample. After characterization, TPD of C^{18}O was studied. To exclude the possibility that ISS might damage/modify the sample, some TPD runs were done without prior ISS. Finally, after TPD analysis, the sample was recharacterized to examine changes in sample stoichiometry, oxidation state, and morphology, induced by the TPD process.

A. X-ray photoelectron spectroscopy

Figure 2 shows the $\text{Ti } 2p$ XPS following different annealing procedures. The expected positions¹⁷ of the $2p_{3/2}$ peaks from different oxidation states of Ti are indicated with vertical dashed lines and the labels 0, +3, and +4. To correct for sample charging, which depends somewhat on preparation conditions, all spectra have been referenced to the $\text{O } 1s$ peak, assumed to be at 530.8 eV as in stoichiometric TiO_2 .¹⁷ As a check on this correction, note that the resulting Ti +4 binding energy is in excellent agreement with the expected value of 459.5 eV. The spectrum labeled $\text{TiO}_{1.44}$ is for the freshly sputtered surface, without annealing. The XPS spectrum shows a broad range of Ti oxidation states ranging from 0 to +4, consistent with preferential sputtering of surface oxygen. The $\text{O } 1s$ XPS peak for this sample is broadened by almost 1 eV compared to the $\text{O } 1s$ XPS for annealed TiO_2 . The broadening suggests that a range of oxygen environments is present in the near-surface region, and also makes the charging correction less precise. The stoichiometry cal-

culated from XPS of the reduced surface is $\text{TiO}_{1.44}$, which is an average over electron escape depth.

When the reduced TiO_2 is annealed in UHV at 900 K for a 1 h, the surface appears to be fully oxidized (spectrum labeled “stoichiometric TiO_2 ”). Both the ratio of Ti and O peak intensities, and the absence of signal for Ti (+3) are consistent with TiO_2 stoichiometry. The oxidation may occur by diffusion of bulk oxygen to the surface as proposed by Lusvardi *et al.*¹⁹ and/or by diffusion of titanium cations from the surface to the bulk as suggested by Henderson.²⁰ Henderson²⁰ and Linsebigler *et al.*,²¹ found that annealing at 900 K creates 5%–10% of oxygen vacancies on the surface, however, their annealing times are much shorter than ours. For short annealing times we also observe significant intensity for Ti (+3), consistent with numerous oxygen vacancies. Nonetheless, our XPS resolution is not high enough to exclude a small Ti (+3) peak buried in the tail of the Ti (+4) peak, and the TPD results indicate that there are, indeed, significant numbers of surface defects.

When the sputtered TiO_2 is annealed for 1 h at 570 K in 10^{-5} Torr of oxygen, the Ti $2p$ XPS (labeled $\text{TiO}_{2.35}$) shows a shoulder extending over the Ti (+3) binding energy, indicating that under these conditions, the reduced Ti is not completely oxidized. The stoichiometry calculated from XPS was $\text{TiO}_{2.35}$, however, indicating that the surface has extra oxygen compared to the UHV-annealed sample. Diebold and co-workers suggested that annealing reduced TiO_2 below 600 K with oxygen exposure of 300 L, oxidizes oxygen vacancy sites but leaves oxygen adatoms bound to the surface.²² A subsequent imaging study from that group showed that atomically flat vacuum-annealed TiO_2 underwent restructuring upon O_2 exposure at elevated temperatures, creating roughened surfaces.²³ Our results, below, show that the O_2 -annealed surface is highly oxidizing, consistent with the presence of chemisorbed oxygen. A few experiments were also performed on a surface with XPS-measured stoichiometry of $\text{TiO}_{2.22}$, prepared by annealing sputtered TiO_2 in O_2 at 700 K. As discussed below, this surface also shows the higher oxidative reactivity attributed to chemisorbed oxygen. Both the lower O:Ti ratio, and reduced reactivity compared to the $\text{TiO}_{2.35}$ surface, are consistent with a lower concentration of chemisorbed oxygen.

Figure 3(a) shows the Ni $2p$ XPS following deposition of Ni_2 , Ni_5 , and Ni_{10} on stoichiometric TiO_2 at different *per atom* impact energies. At 1 eV/atom impact energy, Ni is observed only in its zero oxidation state, indicating that there is no redox chemistry between the deposited nickel and the stoichiometric TiO_2 surface. No oxidation is observed for Ni or Ni_{15} deposition at 1 eV/atom either (not shown). Note that for higher impact energies, we begin to see a peak at higher binding energy (856.0 eV), corresponding to formation of Ni in the +3 oxidation state.¹⁷ For Ni_2 , the nickel oxidation is quite clear for an energy of 10 eV/atom. For Ni_5 , a +3 oxidation state peak only becomes obvious at 20 eV/atom, although there is some sign of a shoulder at 10 eV/atom. For Ni_{10} , there is no sign of oxidation at our highest deposition energy. The data indicate that nickel clusters are chemically stable on the stoichiometric TiO_2 surface, but that redox chemistry can be driven with sufficient impact energy.

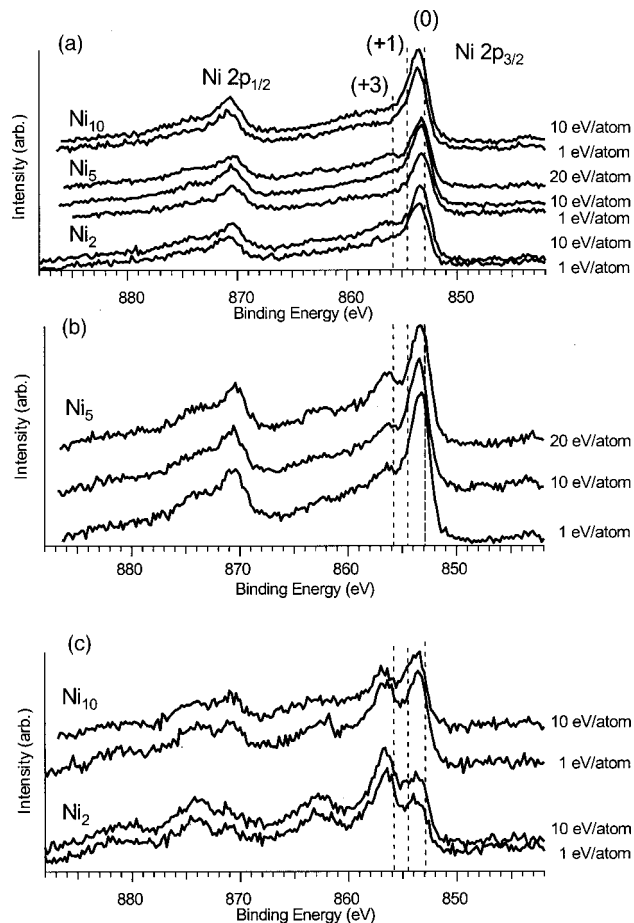


FIG. 3. The Ni $2p$ XPS of the nickel clusters on (a) vacuum annealed TiO_2 ; (b) $\text{TiO}_{2.22}$; and (c) $\text{TiO}_{2.35}$. The numbers to the right of the spectra are the cluster impact energies (eV/atom).

Note that the Ni zero oxidation state XPS peak is shifted towards higher binding energy by ~ 0.4 eV, relative to the dashed line indicating the peak position in metallic Ni. This shift is consistent with studies of Ni binding energy shifts for evaporated Ni/ TiO_2 films, discussed above.^{7,9,10} We also find that the Ti $2p$ XPS broadens slightly to lower binding energy, upon Ni dosing.

Figure 3(b) shows the nickel $2p$ XPS after depositing Ni_5 on $\text{TiO}_{2.22}$. Even at the lowest impact energy, a significant Ni +3 oxidation state peak is observed, indicating that this surface is more oxidizing than the stoichiometric TiO_2 . The comparison clearly shows that Ni oxidation at low impact energy results from nickel interactions with oxygen chemisorbed at defects, rather than with the titania, itself. The observation that only a small fraction of the Ni atoms in Ni_5 are oxidized, suggests that the Ni atoms deposited as clusters are not highly mobile on the surface at room temperature. Otherwise they would be able to scavenge additional chemisorbed oxygen. The ISS results discussed below are consistent with this conclusion. Note that the extent of oxidation increases substantially with impact energy. Because oxidation is also observed on the stoichiometric surface at high impact energies, we attribute the increased oxidation to reaction with titania, rather than an increase in Ni mobility.

Figure 3(c) shows the results of Ni cluster deposition on the $\text{TiO}_{2.35}$ surface, where we believe that there is substantially more chemisorbed oxygen. Consistent with this belief, we observe that a substantially greater fraction of deposited Ni is oxidized. There is a significant cluster size effect in the degree of oxidation. For Ni_2 , even at the lowest deposition energy, roughly 80% of nickel atoms are oxidized, suggesting that there is sufficient chemisorbed oxygen near most impact sites to oxidize the cluster, or possibly that the dimers are sufficiently mobile to scavenge nearby chemisorbed oxygen. For Ni_{10} , approximately 60% of nickel atoms remain in the zero oxidation state, presumably because there is simply not enough active oxygen to fully oxidize the larger cluster. Because the total Ni atom dose is identical in all experiments, the different behavior of Ni_2 and Ni_{10} is another sign that the Ni atoms are not highly mobile at room temperature, at least when deposited as clusters. If diffusion were facile regardless of the form in which the Ni is deposited, we would expect the final state of the system to be cluster size independent. Note that the time scale of the experiments is on the order of one hour (including both deposition and XPS analysis time) while the areal density of chemisorbed oxygen must be quite high to give the $\text{TiO}_{2.35}$ apparent stoichiometry. Evidently the diffusion rate is near zero for Ni deposited as clusters with size on the order of ten atoms.

When Ni clusters are deposited on freshly sputtered TiO_2 , without annealing, only zero oxidation state nickel is observed at all impact energies, presumably because the surface is quite oxygen deficient and Ti has a higher oxygen affinity than Ni. In addition, there is no shift in the zero oxidation state peak.

B. Low energy ion scattering spectroscopy

Further insight into the structure of the sample surfaces, and the effects on the samples of CO adsorption and of heating, can be obtained from low energy ion scattering spectroscopy (ISS). Here, a $^4\text{He}^+$ beam with 1 keV incident energy (E_0) impinges on the surface at 45° incident angle, and the kinetic energy (E) of scattered ions is detected along the surface normal, after scattering by 135° . The dominant scattering process observed in ISS can be regarded as binary elastic collisions between incident He^+ and single atoms on the surface. In that case, the position of peaks, E/E_0 , is simply related to the masses of surface atoms from which the He^+ scatters.²⁴

While ISS peak positions provide unambiguous identification of surface atoms, via their mass, the peak intensities depend on three factors: the cross section for scattering from a particular type of atom, the He^+ ion survival probability (ISP), and the extent to which different surface atoms are shadowed or blocked by other surface atoms. For 1 keV He^+ , the scattering is from the core electrons of the target atoms, and the effective atomic sizes are much smaller than the interatomic spacings. The probability for scattering into our detector is proportional to the square of the impact parameter (b^*) that leads to 135° scattering. These b^* values were estimated by running classical trajectories for an empirically corrected Molière potential.²⁴ The cross sections (σ) are in the ratio, 0.23:1:1.4 for $\sigma_{\text{O}}:\sigma_{\text{Ti}}:\sigma_{\text{Ni}}$.

A major factor in ISS is that most He^+ is neutralized during the scattering process. The ion survival probability (ISP) depends on the electron densities traversed during each scattering trajectory, and varies with the chemical element, oxidation state, and local environment of the target atom. As a consequence, peak intensities in ISS are not simply related to surface concentrations. One simplification resulting from neutralization is that only atoms in the topmost layer contribute significantly to the scattered ion intensity. If Ni is deposited on top of the surface, the Ti or O atoms to which it is bonded are effectively second layer atoms, and the scattering signal from these atoms is expected to be significantly attenuated.

The final effects are blocking and shadowing. Blocking is when He^+ scattered from one atom cannot reach the detector because a second atom is in the way. Because we detect along the surface normal, blocking effects only atoms directly underneath the surface atom, and these second layer atoms already have negligible detection probability. Shadowing refers to the fact that atoms on the surface cast a roughly conical scattering shadow, i.e., scattering from a surface atom prevents He^+ from reaching other atoms that are directly behind it. For 1 keV He^+ scattering from Ni, for example, the shadow cone radius is estimated to be²⁵ $\sim 0.9 \text{ \AA}$ at a distance of 2 \AA . The shadowing effect depends on the angle of incidence, the Ni binding geometry, and the azimuthal angle of the surface with respect to the ion beam. We cannot vary azimuthal angle in our experiment, but measure identical ISS spectra for different samples mounted with random azimuthal angles, verifying that we have not accidentally chosen an azimuthal angle where shadow cone edge effects²⁴ are significant. It is straightforward to estimate the average shadowing per Ni atom on the surface, by simply counting surface atoms within the shadow cone, averaging over azimuthal angle. For our rather steep angle of incidence, it turns out that the shadowing effect is small. For dispersed atoms in the A–D binding sites and for the dimer and pentamer structures in Fig. 1, the shadowing ranges from ~ 0.4 to ~ 0.7 Ti or O atoms shadowed per Ni. Most of these atoms are bound to the Ni, and therefore are expected to have reduced ISP, anyway.

Because of ISP and shadowing effects, the relative intensities of Ni, Ti, and O peaks depend strongly on how the Ni is disposed on the surface. For example, Ni in sites A or B (Fig. 1) would attenuate only O intensity, while Ni in site C or D would effect both O and Ti intensities. In general, the greatest attenuation of Ti and O intensities should occur for Ni dispersed as atoms on top of the surface, because each Ni attenuates He^+ scattering signal from a number of surrounding substrate atoms. With increasing cluster size, we expect that a given dose of Ni will result in less attenuation of O or Ti signal, because a smaller fraction of the substrate surface is covered.

The Ni ISS signal is also important, providing insight into the cluster morphology. As long as all Ni remains in the top layer, the Ni signal should be roughly independent of cluster size. If the Ni forms multilayer particles, however, only the top layer Ni contributes to the Ni ISS, and more TiO_2 surface is exposed. The result would be a substantial

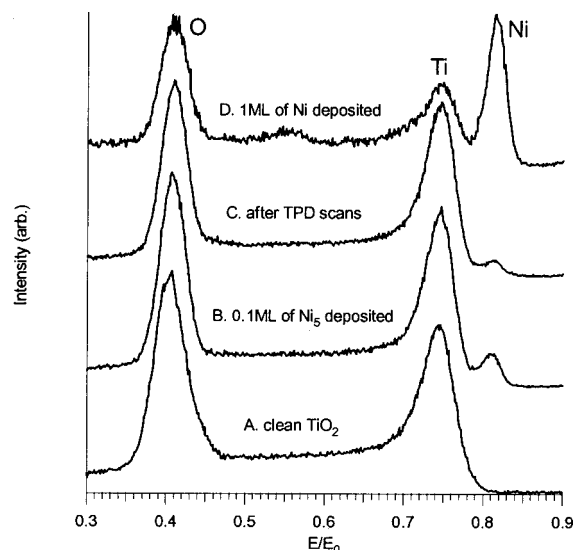


FIG. 4. Typical low energy ion scattering spectra. (A) clean TiO_2 ; (B) TiO_2 with 2.0×10^{14} Ni atoms/ cm^2 (0.1 ML) deposited as Ni_5 at 1 eV/atom; (C) same as (B), after TPD experiments; (D) TiO_2 with 2.0×10^{15} per cm^2 of Ni^+ deposited at 1 eV (1 ML).

decrease in Ni/Ti and Ni/O ratios. Another possibility is strong metal-support interaction (SMSI), i.e., encapsulation of Ni particles by TiO_2 . Recent work of Diebold and co-workers²⁶ provides a textbook example of SMSI, wherein Pt clusters annealed on TiO_2 are completely encapsulated in a reduced TiO_x layer, resulting in complete loss of Pt ISS signal. Encapsulation has been observed for Ni/ TiO_2 , but only following high temperature annealing in a H_2 atmosphere.^{12,27} A related possibility is that the Ni might diffuse into the TiO_2 lattice, forming a mixed oxide phase, in which case, the Ni signal would be strongly attenuated. Finally, at our highest deposition energies, it is not impossible that some Ni implantation into the TiO_2 surface might occur. Such implantation would result in strong attenuation of Ni ISS signal.

Figure 4 shows a number of ISS spectra, and Table I gives ratios of peak intensities. Trends with cluster size are summarized in Fig. 5. Ratios are reported, rather than raw intensities, because the data were taken over a several month period, and it is impossible to keep the He^+ beam parameters exactly constant from run to run. Also included in the table for comparison, are data for deposition of 0.1 ML and 1.0 ML of Ni^+ at 1 eV.

Before considering the ISS data for the clusters, it is useful to consider two limiting cases. Figure 4(A) shows an ISS spectrum of clean TiO_2 , prior to Ni deposition. The O/Ti intensity ratio is 1.27, consistent with the results of Diebold and co-workers.²⁶ The ratio expected in absence of ISP effects is only 0.69, estimated as the product of $\sigma_{\text{O}}/\sigma_{\text{Ti}}$ ($=0.23$) and the relative number of first layer O and Ti atoms (3:1). The fact that the measured O/Ti ratio is substantially larger indicates that the ISP is lower for scattering from Ti than for scattering from O, probably reflecting the more exposed geometry of O on this surface (Fig. 1).

The other interesting point of comparison is the experiment where 1.0 ML of Ni^+ was deposited at 1 eV [Fig.

TABLE I. ISS intensity ratios, and integrated intensities.

Sample	Cluster	Energy	O/Ti ratio	Ni/substrate ratio ^a
Clean TiO_2			1.27	
0.1 ML, before TPD	Ni	1 eV	0.98	0.07
	Ni_2	1 eV	0.98	0.08
		10 eV	0.90	0.06
	Ni_5	1 eV	1.12	0.07
		10 eV	1.10	0.08
	Ni_{10}	1 eV	1.24	0.08
10 eV		1.29	0.12	
		1.36	0.01 ₄	
1 ML, before TPD	Ni	1 eV	1.75	1.07
0.1 ML, after TPD	Ni	1 eV	1.0	0.03
		1 eV	0.90	0.02
	10 eV	0.94	0.02	
		0.98	0.02	
	10 eV	not taken		
		1.13	0.04	
	10 eV	0.81	0.04	
		1.34	0.01 ₂	
	1 ML, after TPD	Ni	1 eV	1.73

^aAverage of Ni/O and Ni/Ti ratios. Where given, the subscripted final digits are given only to show the trend.

4(D)]. Under this condition, the Ni, O, and Ti peaks are all comparable in size, and the O/Ti ratio is 1.75. As noted in the Introduction, there is some debate in the literature about the growth mechanism for Ni evaporated onto $\text{TiO}_2(110)$, with some data suggesting that growth is initially layer-by-layer, and other data indicating three-dimensional growth from the

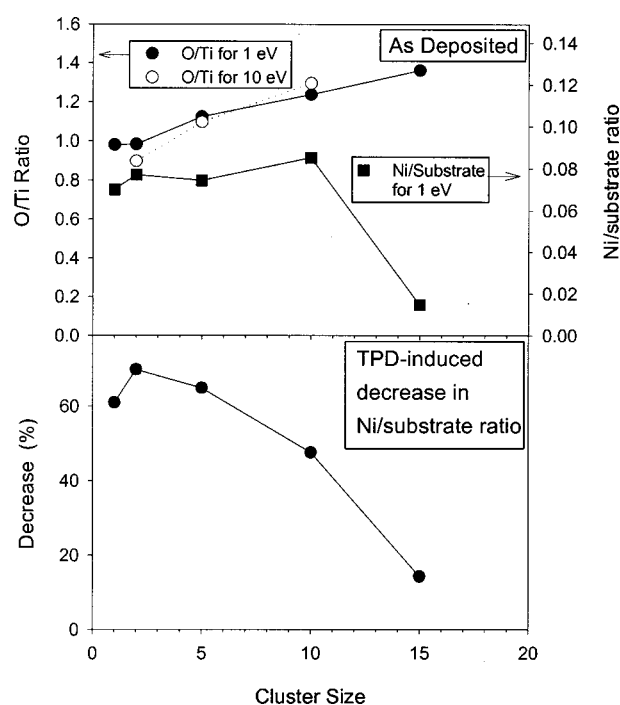


FIG. 5. Top frame: O/Ti ISS ratios (left-hand scale) and Ni/substrate ISS ratios (right-hand scale) for as-deposited Ni and Ni clusters on TiO_2 at a constant dose of 0.1 ML of Ni atoms. Bottom frame: Percent decrease in Ni/substrate ISS ratio induced by TPD, as a function of cluster size.

start. The ISS results indicate that for our conditions, the growth mechanism is 3D to some extent. This conclusion rests on the observation of Ti and O ISS intensities $\sim 64\%$ and 50% of those for clean TiO_2 . If growth were entirely two-dimensional, our $2.0 \times 10^{15} \text{ Ni/cm}^2$ dose would completely block the O and Ti ISS. On the other hand, it appears that the degree of Ni agglomeration is not high, as shown by both the strong Ni ISS signal and the observation of substantial attenuation of substrate ISS signal. If large multilayer particles were forming, for example, then we would expect less attenuation of the Ti and O signals, and the Ni signal would be weak, because only the top layer Ni atoms would be observable. Limited agglomeration is not surprising given the strong and highly corrugated Ni– TiO_2 binding calculated by Pala *et al.*⁶

When 0.1 ML equivalents of Ni, Ni_2 , Ni_5 [Fig. 4(B)], Ni_{10} , and Ni_{15} are deposited at 1 eV/atom, the O/Ti ratios are 0.98, 0.98, 1.12, 1.24, and 1.36, respectively (Fig. 5, top frame). The large drop in O/Ti ratio for Ni and Ni_2 , relative to clean TiO_2 , indicates that Ni attenuates scattering signal from O more than Ti, suggesting that binding is preferentially to oxygen sites. This result is consistent with the calculations of Pala *et al.*⁶ indicating that oxygen binding is energetically preferred for Ni atoms. The fact that the ratio is identical for Ni and Ni_2 is not surprising. Regardless of how they land, Ni atoms should be able to settle into the more stable oxygen binding sites (A or B, Fig. 1). Ni_2 can presumably bind with each atom in an adjacent A site, or at least with both atoms in adjacent oxygen sites (Fig. 1). In either case, the ISP and shadowing/blocking effects attenuate scattering from O, but not Ti. The observation that the O/Ti ratio increases with deposited cluster size, is also not unexpected. Larger clusters cover less of the surface, leading to more contribution from bare TiO_2 regions, and because large clusters have large footprints, they necessarily attenuate scattering from both Ti and O. It may seem surprising that the ratio can exceed that for clean TiO_2 , however, we note that the ratio is 1.75 for the 1.0 ML Ni sample. Without knowing the details of how clusters bind to the surface, and how cluster binding might modify the ISP for scattering from neighboring atoms, it is not possible to interpret the O/Ti ratios quantitatively. Nonetheless, the trends suggest that the average size of Ni clusters on the surface is correlated with the size of the deposited clusters. The O/Ti ratios clearly rule out substantial fragmentation or agglomeration of the clusters, because in that case, the ratio should be roughly size-independent. Furthermore, we can rule out certain binding arrangements. For example, if deposited clusters rearranged from the compact geometry of gas-phase Ni clusters,^{28,29} to a linear cluster bound along a row of oxygen atoms (e.g., bound to neighboring “A” sites), then the O/Ti ratio would remain near that for isolated atoms, independent of cluster size.

The Ni/substrate ISS ratios (i.e., Ni/Ti and Ni/O) provide additional morphological insight, summarized in Table I and the top frame of Fig. 5. As comparison of curves B and C of Fig. 4 indicates, the dominant factor effecting the Ni/substrate ratios is changes in the Ni ISS intensity, although the individual Ni/Ti and Ni/O ratios obviously also reflect the

changes in the O/Ti ratio discussed above. To isolate the trends in the Ni ISS signal from the changes in O/Ti ratios, Table I and Fig. 5 give Ni/substrate ratios, taken as the average of the Ni/O and Ni/Ti ratios. The Ni/substrate ratios depend on the fraction of deposited Ni atoms exposed on the surface, along with the ISP for scattering from those atoms. As already noted, sintering into multilayer particles or penetration of Ni into the surface would result in substantial decrease in the Ni signal. For Ni, Ni_2 , Ni_5 , and Ni_{10} , the nearly constant Ni/substrate ratios suggests that most or all Ni remains in the top layer. For Ni_{15} , however, the Ni intensity is substantially lower, consistent with this large cluster retaining a three-dimensional structure on the surface, where scattering from most of the Ni atoms is attenuated by the presence of a few top layer Ni atoms.

When the deposition energy is increased to 10 eV/atom, the O/Ti ratios remain approximately constant, suggesting that the Ni dispersion on the surface is not grossly altered at high impact energies. If clusters were shattering in high energy deposition, for example, the O/Ti ratios would drop to near the small cluster limit (<1). There are signs in the Ni/substrate ratios, however, that the cluster structures are affected by increased deposition energy. For Ni_2 , the Ni/O and Ni/Ti ratios decrease by $\sim 25\%$, suggesting that some Ni is being driven into the TiO_2 substrate. We would expect these implanted Ni atoms to be oxidized, and indeed, our XPS results [Fig. 3(a)] show significant oxidation for Ni_2 at 10 eV/atom. The alternative explanation, that Ni sticking probability is reduced at high impact energies, is ruled out by the observation that the total Ni XPS intensity does not decrease for deposition at high energies.

For Ni_5 and Ni_{10} no oxidation is observed in the XPS at 10 eV/atom, consistent with the observation of no decrease in Ni/O or Ni/Ti ratios. For Ni_{10} , in fact, there is a small *increase* in Ni ISS signal, reflected in both the raw intensities and the ratios. A not unreasonable explanation for this effect is that at low impact energies, the deposited Ni_{10} retains, to a small degree, the 3D structure of the free cluster. At 10 eV/atom, more flattening of the cluster is expected, exposing more Ni to the ion beam.

In summary, the ISS results for the as-deposited clusters are consistent with the clusters remaining approximately intact on the surface, particularly at low deposition energies. The larger clusters probably even retain some 3D structure. We certainly are not suggesting that the cluster structures are unperturbed by the impact process or by binding to the surface. Indeed, the strong (and highly corrugated) binding calculated by Pala *et al.*⁶ for Ni atoms on TiO_2 suggests that cluster structure is undoubtedly effected even for low impact energies, but at the same time, the tendency to diffusion is reduced.

ISS was measured for each sample following the sequence of TPD experiments described below, and the results are given in the bottom half of the table and summarized in the bottom frame of Fig. 5. Particularly for the smaller clusters, the ISS results show that there are large changes in the morphology of the deposited nickel, induced by the CO adsorption, heating, and desorption that occurs in TPD. The Ni signal drops significantly after TPD, as shown for Ni_5 by

comparison of traces B and C in Fig. 4. The decreases in Ni/substrate ratio for Ni, Ni₂, Ni₅, Ni₁₀, and Ni₁₅, are 61%, 70%, 65%, 47%, and 12%, respectively (Fig. 5). For the 1 ML Ni deposit, a decrease of 29% is observed. The effect is similar for deposition at 1 eV/atom and 10 eV/atom, again suggesting that cluster properties are not grossly perturbed by deposition energy in this range. In XPS, we observe little TPD-induced change in the Ni 2*p* intensity, and no Ni-containing species are observed to desorb during TPD. These observations indicate that Ni remains in the near-surface layers after TPD. The XPS data indicate a small increase in the fraction of Ni in the +3 oxidation state, but >90% remains in the zero oxidation state.

The decreases in the Ni ISS signal must, therefore, be interpreted in terms of changes in Ni morphology during TPD. There are two limiting case mechanisms. Ni might be sintering into multilayer particles, in which a significant fraction of the Ni atoms are no longer in the ISS-accessible top-layer. Alternatively, it might be that SMSI results in partial encapsulation of the Ni clusters in TiO₂. (We can rule out complete encapsulation because the substantial Ni ISS signal is still observed.) In principle, it should be possible to distinguish sintering from partial encapsulation by the differing extents of XPS signal reduction that would result. To test this idea, we did simple continuum electron attenuation calculations³⁰ for two model morphologies, using inelastic mean free path values for Ni and TiO₂ from the NIST database.¹⁸ The XPS signal reduction calculated for a two layer Ni deposit (which would give ISS attenuation of 50%), is ~8% relative to Ni in a single layer. This reduction is essentially identical to the ~7% reduction calculated for a model single layer Ni deposit with 50% coverage of a single layer of TiO₂.

Both sintering and partial encapsulation mechanisms are consistent, within the experimental uncertainty, with the ~6% percent decrease observed in the XPS following TPD. Several considerations favor the sintering mechanism, however. Sintering would explain why the reduction in Ni ISS signal is inversely dependent on cluster size. Large clusters tend to be more stable with respect to surface diffusion than small clusters, and thus are expected to sinter less. The small reduction observed for Ni₁₅ is also consistent with a sintering mechanism, because the ISS data suggest that as-deposited Ni₁₅ is already three-dimensional. Sintering has been observed for Ni/TiO₂ at elevated temperatures by STM.⁸ Finally, it seems likely that encapsulation of our small nascent clusters would lead to a significant degree of Ni oxidation, not observed in the post-TPD XPS. It must be noted, however, that we cannot rule out the partial encapsulation mechanism, which could account for the observations if it is assumed that the tendency toward encapsulation is inversely dependent on cluster size, and if encapsulation is not accompanied by oxidation, even of atoms and dimers.

We did one experiment bearing on the sintering/encapsulation question. For a freshly-deposited Ni_n/TiO₂ sample, the Ni ISS signal is observed to decrease monotonically with time under the He⁺ beam, because the Ni is slowly sputtered away. After a TPD experimental cycle, the Ni signal is still observed to decrease monotonically with

time. If the TPD-induced decrease in the Ni ISS signal were attributable to partial encapsulation by TiO_x, we might expect that the Ni ISS signal would initially increase with time, because sputtering of the TiO_x overlayer would tend to expose additional Ni.

The one observation that is hard to reconcile with a pure sintering model, is that the O/Ti ratios do not increase significantly following a TPD cycle, as might be expected from the trend in O/Ti ratio with increasing size of deposited cluster. We looked for loss of oxygen from the surface as both O₂ and CO₂, but none is observed in the temperature range of the TPD experiments. One possibility is that the mechanism includes both sintering and SMSI, i.e., Ni may be sintering into larger particles, but there may also be some SMSI at the interface between the Ni particle edges and the support. By bringing some partially reduced TiO_x to the surface, SMSI would reduce the O/Ti ratio.

C. Temperature-programmed desorption

TPD experiments were performed for Ni clusters deposited on stoichiometric TiO₂(110). The sample was cooled by conduction to a liquid N₂ reservoir to an initial temperature of ~140 K. The sample was then dosed with a saturation dose of C¹⁸O (>20 L). Prior to each TPD heating run, the filament used for electron-bombardment heating was flash-heated for 0.5 s with the electron bias voltage set to 300 V. This desorbs CO from the area around the heater, and also removes CO from surfaces where electron-stimulated desorption might cause elevated background during the TPD run. All TPD were done at a constant 3 K/s heating rate, followed by rapid cooling. The quadrupole mass spectrometer was rapidly switched between masses of interest during the heating phase of the experiment. In each run we monitor C¹⁸O⁺, Ni⁺, C¹⁶O¹⁸O⁺, and C¹⁸O₂⁺. Ni⁺ is monitored because this is the major nickel-containing ion observed in electron bombardment ionization of nickel carbonyl.³¹

Figure 6 shows C¹⁸O TPD spectra for several surfaces of interest for comparison with the Ni_n/TiO₂ samples. For these samples, no desorption of Ni-containing species or CO₂ is observed. The top frame shows the result for CO TPD from clean stoichiometric TiO₂(110), with no Ni cluster deposition. Based on TiO₂ CO TPD results in the literature,²¹ the CO desorption peak for perfect TiO₂(110) under our TPD conditions should be at ~130 K. The ~140 K starting temperature achievable with our transferable sample holders is, therefore, too high to see the main CO desorption peak. In the literature TPD results, for TiO₂ with annealing history similar to ours, a high temperature tail of CO desorption from TiO₂ defect sites is observed, to almost 350 K. We, therefore, attribute the desorption feature observed in our TPD spectrum to CO desorption from defect sites on the surface.

The middle frame shows TPD from single crystal Ni(100), following a ~20 L CO dose at 220 K. A peak is observed at ~420 K, with a shoulder at ~320 K. For a dose about six times lower, the low temperature shoulder disappears. This structure and dose dependence is consistent with the recent detailed TPD study of Muscat and Madix³² which

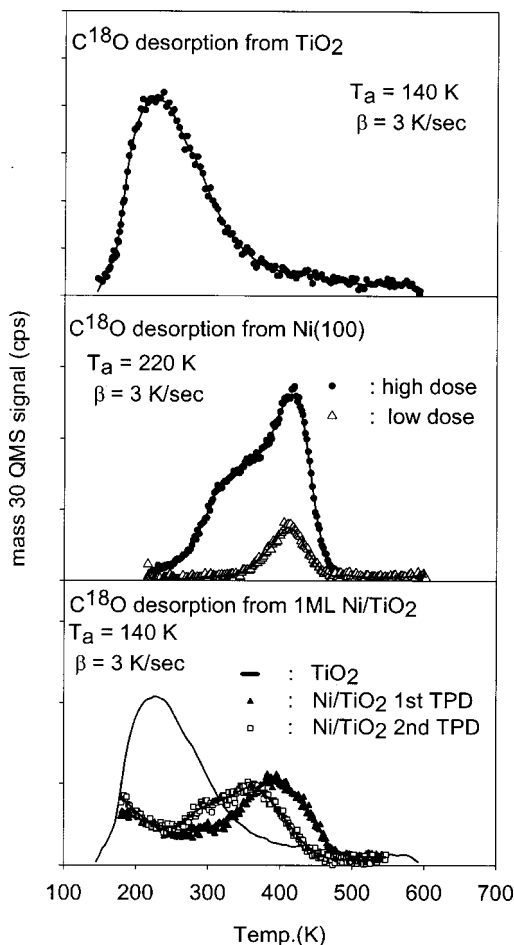


FIG. 6. $C^{18}O$ TPD spectra for comparison with cluster results. Top: Desorption following saturation dose on clean TiO_2 . Middle: Desorption from $Ni(100)$ at saturation dose, and a dose ~ 6 times lower. Bottom: Desorption from sample prepared by deposition of $2.0 \times 10^{15} Ni^+/cm^2$ (1 ML Ni) on TiO_2 , showing changes between first and second TPD scans, and TPD for clean TiO_2 , for comparison.

showed clearly that a succession of more weakly bound states is filled as CO dose is increased.

The final frame shows an experiment designed for comparison with the study of Raupp and Dumesic.¹² In their study, Ni films were evaporated onto an oxidized polycrystalline Ti surface, then subjected to TPD after various substrate and Ni annealing procedures. In the experiment closest to ours, they deposited 0.2 nm of Ni (~ 1 ML) then did CO TPD with no other pretreatment. In our experiment, we deposited a monolayer ($2.0 \times 10^{15} Ni/cm^2$) as atomic ions at an impact energy of 1 eV. The ISS results indicate that our Ni is aggregating to a limited extent upon deposition at room temperature, leaving about half the TiO_2 surface free of Ni. We measured two sequential TPD runs, in each run cooling the sample, applying a saturation CO dose, then ramping the temperature at 3 K/s to 600 K. The first TPD run, with as-deposited Ni, resulted in a broad peak at 385 K, almost identical to that observed by Raupp and Dumesic for 0.2 nm Ni on fully oxidized titanium. In our second TPD run, the peak broadened and shifted to lower temperature, with a hint of a second peak near 300 K. The ISS results, where the Ni/substrate ratio decreases by 29% following a single TPD

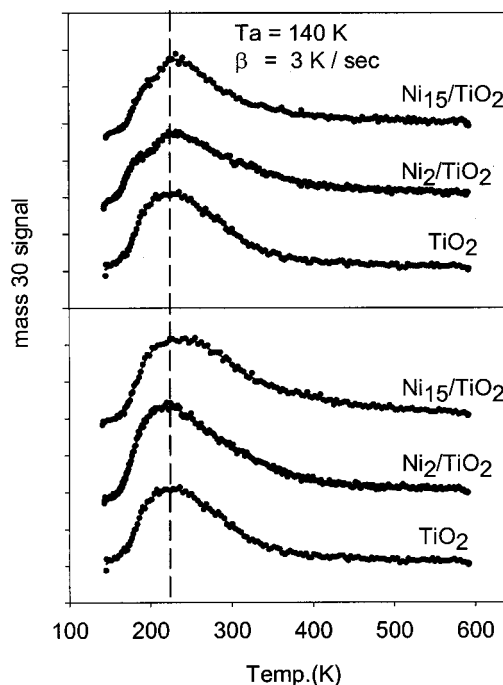


FIG. 7. $C^{18}O$ TPD clean TiO_2 , and from Ni_2 and Ni_{15} supported on vacuum annealed TiO_2 . Top: First TPD run. Bottom: Second TPD run, showing loss of structure.

cycle, suggests that sintering and/or partial encapsulation take place during TPD. Although the conditions were somewhat different, a similar trend was observed by Raupp and Dumesic.

Figure 7 shows $C^{18}O$ TPD spectra run under identical conditions for clean TiO_2 , and TiO_2 with $2.0 \times 10^{14} Ni$ atoms/ cm^2 , deposited as Ni_2^+ , and Ni_{15}^+ at 1 eV/atom deposition energy. The other size clusters and deposition energies give similar results. No mass spectral signal was observed for Ni^+ , $C^{18}O_2^+$, or $C^{16}O^{18}O^+$, consistent with XPS indications that the stoichiometry of the near-surface region is not altered by CO TPD. In particular, there is no carbon build-up following TPD. The most obvious point is that there is little change in the TPD due to Ni_n deposition. In the spectra for Ni_2 and Ni_{15} , there is some hint of a shoulder near 190 K, and the high temperature tail extends to somewhat higher temperatures than for the clean TiO_2 . The shoulder structure, though weak, is reproducible. The lower frame of the figure compares the results of a second, sequential TPD run from each sample. Note that the weak shoulder structure observed in the first run is absent.

Several conclusions can be drawn from this result. First, CO binding to small Ni clusters on the surface in low doses is substantially weaker than for the clusters that form in high dose Ni deposition. Whether this is a cluster size effect or an effect of Ni dose-dependent modification of electronic properties is unclear, because it is not known what cluster size distribution forms in the high dose Ni deposition. The ISS results, above, indicate that the TPD cycle of adsorption/desorption and heating leads to substantial sintering and/or encapsulation of the very small clusters ($n=2,5$), with less change observed for Ni_{10} , and little for Ni_{15} . Presumably this TPD-induced effect leads to the loss of the weak shoul-

der structure in the second TPD run. Apparently sintering under these conditions does not lead to growth of large Ni clusters that would have significantly increased CO desorption temperatures, perhaps approaching that of bulk Ni (~ 400 K).

The STM work of Tanner *et al.*⁸ provides a useful point of comparison. In their experiment, nickel atoms were evaporated onto a TiO₂(110) support, and the resulting clusters were imaged. For a dose of 2×10^{14} atoms/cm² at a substrate temperature of 375 K, dome-shaped 1.6 nm diam clusters were obtained. From the reported contact angle, we can estimate that these clusters contain only about 30 atoms. Our cluster dose is about the same, and while we heat to 600 K in our TPD runs, the total time at temperatures above 375 K is < 2 min. If the TPD-induced sintering of our small clusters stopped in the 30 atom size range, that would explain several observations. First, the Raupp and Dumesic work suggests that for larger Ni particles on TiO₂, CO desorption peaks should be observed at higher temperatures, as in our 1 ML Ni⁺ experiment. No such peaks are observed in repeated TPD experiments, suggesting that large particles do not grow for the 0.1 ML dose of Ni. Stopping in the 30 atom size range would also explain why the TPD-induced changes in Ni ISS signal are large for Ni₂ and Ni₅, but smaller for Ni₁₀ and especially Ni₁₅. For the small clusters, sintering into multilayer particles leads to a large decrease in the fraction of Ni atoms exposed in the top layer. For Ni₁₅, where the as-deposited structure appears three-dimensional, sintering into a 30 atom cluster would result in only a small change in the fraction of exposed Ni.

We also considered the possibility that CO adsorption might be breaking up the clusters into isolated metal surface carbonyls, which then desorb CO at low temperatures. The nickel would have to reaggregate into clusters during the course of TPD, because the ISS data are inconsistent with increased Ni dispersion following TPD. Because we are not currently able to do ISS/XPS with the sample at low temperatures, we cannot completely eliminate this possibility, but it seems unlikely. In order that we not see CO desorption at high temperatures, the CO–Ni binding must be weak, and in that case, CO adsorption would be unlikely to result in cluster disruption. We did look at XPS and ISS of Ni_n/TiO₂ exposed to a saturation dose of CO at room temperature. No carbon was detected by XPS, and the Ni/O and Ni/Ti ISS ratios were not altered from the values prior to the CO dose. One could argue that we might not see a small coverage of CO by its C 1s XPS signal, but CO binding to Ni atoms would certainly attenuate the Ni ISS signal. It seems clear from this result that at room temperature, CO is not sticking to the Ni in the Ni_n/TiO₂ sample. Furthermore, the lack of change in ISS suggests that CO adsorption/desorption at room temperature does not significantly modify the clusters.

While it is clear that the CO binding is weak for our small clusters, the question is why. The work of Riley and co-workers^{29,33} clearly shows that CO binds to gas-phase Ni_n in our size range, and the results of Heiz and co-workers^{2,34} for Ni_n/MgO indicate that Ni–CO binding is reasonably strong in that system. This comparison suggests that the weak CO binding for low dose Ni/TiO₂ is a consequence of

strong interaction with the support. We observe no desorption of nickel carbonyls for Ni_n/TiO₂, whereas this is a major TPD channel for the Ni_n/MgO ($n < 4$). In addition, CO is observed to bind both molecularly and dissociatively on Ni_n/MgO ($n > 10$), with TPD peaks at ~ 240 and ~ 600 K, respectively, while no dissociative adsorption is observed for Ni/TiO₂. We note that DFT calculations indicate nickel atom binding energies are ~ 1 eV for MgO (Refs. 35, 36) and ~ 2.6 eV for TiO₂.⁶ The stronger binding on TiO₂ presumably results in a concomitant weakening of the CO–Ni binding energies, consistent our observation that CO binding to Ni is comparable to, or weaker than the binding to defects on the TiO₂ surface. Stronger Ni-support binding probably also accounts for our not seeing desorption of nickel-containing species for Ni_n/TiO₂—the Ni–TiO₂ binding is much stronger than the CO–Ni binding, so that CO cannot volatilize even small Ni clusters. In the Heiz experiments, they have no direct means for examining cluster morphology changes induced by CO adsorption/desorption. Given that we see substantial TPD-induced sintering for Ni/TiO₂, we would expect extensive TPD-induced sintering in the more weakly bound Ni_n/MgO system, and possibly some diffusion/sintering at room temperature.

ACKNOWLEDGMENTS

Development of the instrumentation and the experiments reported were supported by the Air Force Office of Scientific Research (F49620-00-1-0138), and the Department of Energy, Office of Science, Basic Energy Science Program, under Grant No. DEFG0399ER15003. Support does not constitute endorsement by DOE of the views expressed herein. Development of the instrument was also supported by a seed grant from the University of Utah, and an equipment donation from Kodak, Inc. Rajganesh Pala from Professor Thanh Truong's group (University of Utah) provided prepublication results of his calculations on Ni/TiO₂ binding and useful discussions regarding bonding to TiO₂. The authors are grateful for many discussions with Professor Jihwa Lee from Seoul National University, and Professor Kevin Boyd from the University of New Orleans.

¹F. Vanolli, U. Heiz, and W.-D. Schneider, *Chem. Phys. Lett.* **277**, 527 (1997).

²U. Heiz, *Appl. Phys. A: Mater. Sci. Process.* **A67**, 621 (1998).

³U. Heiz, F. Vanolli, A. Sanchez, and W. D. Schneider, *J. Am. Chem. Soc.* **120**, 9668 (1998).

⁴U. Heiz and W.-D. Schneider, in *Metal Clusters at Surfaces*, edited by K.-H. Meiwes-Broer (Springer, Berlin, 2000), p. 237.

⁵U. Heiz and W.-D. Schneider, *Crit. Rev. Solid State Mater. Sci.* **26**, 251 (2001).

⁶R. Pala, F. Liu, and T. Truong (unpublished).

⁷H. Onishi, T. Aruga, C. Egawa, and Y. Iwasawa, *Surf. Sci.* **233**, 261 (1990).

⁸R. E. Tanner, I. Goldfarb, M. R. Castell, and G. A. D. Briggs, *Surf. Sci.* **486**, 167 (2001).

⁹V. Vijayakrishnan and C. N. R. Rao, *Surf. Sci.* **255**, L516 (1991).

¹⁰C. C. Kao, S. C. Tsai, M. K. Bahl, Y. W. Chung, and W. J. Lo, *Surf. Sci.* **95**, 1 (1980).

¹¹J. P. Espinós, A. Fernández, and A. R. González-Elipe, *Surf. Sci.* **295**, 402 (1993).

¹²G. B. Raupp and J. A. Dumesic, *J. Catal.* **97**, 85 (1986).

¹³K. J. Boyd, A. Lapicki, M. Aizawa, and S. L. Anderson, *Nucl. Instrum. Methods Phys. Res. B* **157**, 144 (1999).

- ¹⁴A. Lapicki, K. J. Boyd, and S. L. Anderson, *J. Vac. Sci. Technol. A* **18**, 2603 (2000).
- ¹⁵U. Heiz, F. Vanolli, L. Trento, and W. D. Schneider, *Rev. Sci. Instrum.* **68**, 1986 (1997).
- ¹⁶D. A. Shirley, *Phys. Rev. B* **5**, 4709 (1972).
- ¹⁷*Handbook of X-Ray Photoelectron Spectroscopy*, edited by J. F. Moulder, W. F. Stickle, P. E. Sobol, K. D. Bomben, J. J. Chastain, and R. C. King (Physical Electronics, Eden Prairie, MN, 1995).
- ¹⁸C. J. Powell and A. Jablonski, *NIST Electron Inelastic-Mean-Free-Path Database—Version 1.1* (National Institute of Standards and Technology, Gaithersburg, MD, 2000).
- ¹⁹V. S. Lusvardi, M. A. Barteau, J. G. Chen, J. Eng, Jr., A. Teplyakov, and B. Fruhberger, *Surf. Sci.* **397**, 237 (1998).
- ²⁰M. A. Henderson, *Surf. Sci.* **419**, 174 (1999).
- ²¹A. Linsebigler, G. Lu, and J. T. Yates, Jr., *J. Chem. Phys.* **103**, 9438 (1995).
- ²²W. S. Epling, C. H. F. Peden, M. A. Henderson, and U. Diebold, *Surf. Sci.* **412/413**, 333 (1998).
- ²³M. Li, W. Hebenstreit, L. Gross, U. Diebold, M. A. Henderson, D. R. Jennison, P. A. Schultz, and M. P. Sears, *Surf. Sci.* **437**, 173 (1999).
- ²⁴P. G. Bertrand and J. W. Rabalais, in *Low Energy Ion-Surface Interactions*, edited by J. W. Rabalais (Wiley, Chichester, 1994), pp. 55–116.
- ²⁵O. S. Oen, *Surf. Sci.* **131**, L407 (1983).
- ²⁶O. Dulub, W. Hebenstreit, and U. Diebold, *Phys. Rev. Lett.* **84**, 3646 (2000).
- ²⁷S. Takatani and Y.-W. Chung, *J. Catal.* **90**, 75 (1984).
- ²⁸E. K. Parks, B. J. Winter, T. D. Klots, and S. J. Riley, *J. Chem. Phys.* **94**, 1882 (1991).
- ²⁹E. K. Parks, K. P. Kerns, and S. J. Riley, *J. Chem. Phys.* **112**, 3384 (2000).
- ³⁰A. Lapicki, K. J. Boyd, M. Aizawa, M. Popescu, and S. L. Anderson, *J. Vac. Sci. Technol. A* (submitted).
- ³¹S. E. Stein, director, in *NIST Chemistry WebBook, NIST Standard Reference Database Number 69*, edited by W. G. Mallard and P. J. Linstrom, NIST Mass Spec Data Center, National Institute of Standards and Technology, Gaithersburg, MD 20899 (<http://webbook.nist.gov>), 2000.
- ³²A. J. Muscat and R. J. Madix, *J. Phys. Chem.* **100**, 9807 (1996).
- ³³K. P. Kerns, E. K. Parks, and S. J. Riley, *J. Chem. Phys.* **112**, 3394 (2000).
- ³⁴U. Heiz, R. Sherwood, D. M. Cox, A. Kaldor, and J. T. Yates, Jr., *NATO ASI Ser., Ser. C* **465**, 37 (1995).
- ³⁵A. Markovits, M. K. Skalli, C. Minot, G. Pacchioni, N. Lopez, and F. Illas, *J. Chem. Phys.* **115**, 8172 (2001).
- ³⁶I. Yudanov, G. Pacchioni, K. Neyman, and N. Roesch, *J. Phys. Chem. B* **101**, 2786 (1997).